2018 IEEE/RSJ International Conference on Intelligent Robots and Systems (IROS)
Madrid, Spain, October 1-5, 2018

Liquid Metal-Microelectronics Integration for a Sensorized Soft Robot Skin

Tess Hellebrekers[1], Kadri Bugra Ozutemiz[2], Jessica Yin[2], and Carmel Majidi[1,2]

***Abstract*— Progress in soft robotics depends on the integration of electronics for sensing, power regulation, and signal processing. Commercially available microelectronics satisfy these functions and are small enough to preserve the natural mechanics of the host system. Here, we present a method for incorporating microelectronic sensors and integrated circuits (ICs) into the elastomeric skin of a soft robot. The thin stretchable skin contains various solid-state electronics for orientation, pressure, proximity, and temperature sensing, and a microprocessor. The components are connected by thin-film copper traces wetted with eutectic gallium indium (EGaIn), a room temperature liquid metal alloy that allows the circuit to maintain conductivity as it deforms under mechanical loading. In this paper, we characterize the function of the individual sensors in air and water, discuss the integration of the microelectronic skin with a shape-memory actuated soft gripper, and demonstrate the sensorized soft gripper in conjunction with a 4 degree-of-freedom (DOF) robot arm.**

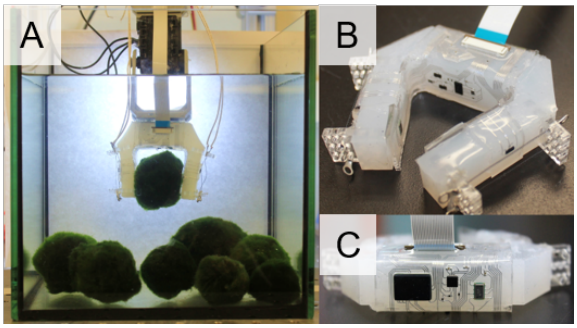

Fig. 1. A) Sensorized soft gripper holding onto medium-sized moss ball inside a water tank. B) Close-up view of sensorized soft gripper with the liquid metal traces and shape-memory coils visible. C) Close-up view of liquid metal traces with processor, IMU, and depth sensors visible.

I. INTRODUCTION

Inspired by the versatility and multi-functionality of biological systems, the field of soft robotics has emerged to address the limitations of rigid robots and machines [1]–[5]. Unlike their conventional rigid counterparts, soft robots utilize gels, elastomers, and fluids as replacements for rigid parts and materials [6], [7]. This allows soft robots to operate under bending, stretching, and compression [8] without losing functionality. These materials have mechanical and rheological properties that are similar to those of biological tissues and, as a result, have become increasingly popular in healthcare robotics [9], human-robot interactions [10], and other delicate tasks [11]. However, in order to achieve complex tasks, a soft robot system requires components for sensing and digital processing that are embedded in its soft elastomer body. Depending on the task at hand, a soft robot may require a wide range of sensing modalities to determine both the environmental state (e.g. shape of the object to be grasped, distance to the object) and the internal state (e.g. orientation). In addition, the system may need on-board digital processing capabilities to control or preprocess incoming raw sensor data. In contrast to rigid robots, the sensing and processing systems on a soft robot must continue functioning despite mechanical deformation while minimizing interference with the underlying mechanics of the host system.

In previous work, we demonstrated a method to reliably interface rigid surface-mount integrated circuits (IC) to liquid metal traces in order to fabricate hybrid stretchable circuits [12]. These hybrid circuits maintain electrical functionality under mechanical deformation while harnessing the reliability and digital capabilities of commercially-available microelectronics. The current paper scales up the fabrication technique for a large detailed circuit design, integrates high-density interconnect patterns, and introduces an on-board processor. Furthermore, we demonstrate a technique to integrate the stretchable sensing skin with a shape-memory actuated soft gripper (Figure 1). Our goals in this study are to: (i) integrate a soft robotic testbed with a soft and stretchable sensing skin that includes an embedded barometric chip, temperature sensor, inertial measurement unit (IMU), time-of-flight range (ToF) chip, and an on-board processor; (ii) characterize and demonstrate the function of the gripper and integrated sensors in air and water; and (iii) demonstrate the performance of the sensorized soft gripper mounted onto a four degree-of-freedom (DOF) robotic arm.

II. RELATED WORK

With the growing popularity of wearables, compliant and stretchable sensing electronics are in increasing demand to sense a diverse amount of stimuli, rapidly transmit data, and process these signals. One approach to achieving stretchable functionality is to use intrinsically soft and deformable conductive polymers and composites [13]–[16] as conductive traces. Another way of achieving stretchability is through

*This work was in part supported by ONR Grants N00014-16-2301 and N00014-14-10778, Code 34, Bio-Inspired Autonomous Systems (PM: Tom McKenna) as well as by the National Science Foundation Graduate Research Fellowship Program under Grant No. DGE 1252522. Any opinions, findings, and conclusions or recommendations expressed in this material are those of the author(s) and do not necessarily reflect the views of the National Science Foundation.

[1]Robotics Institute, School of Computer Science, Carnegie Mellon University, Pittsburgh PA 15123, USA

[2]Department of Mechanical Engineering, Carnegie Mellon University, Pittsburgh PA 15123, USA

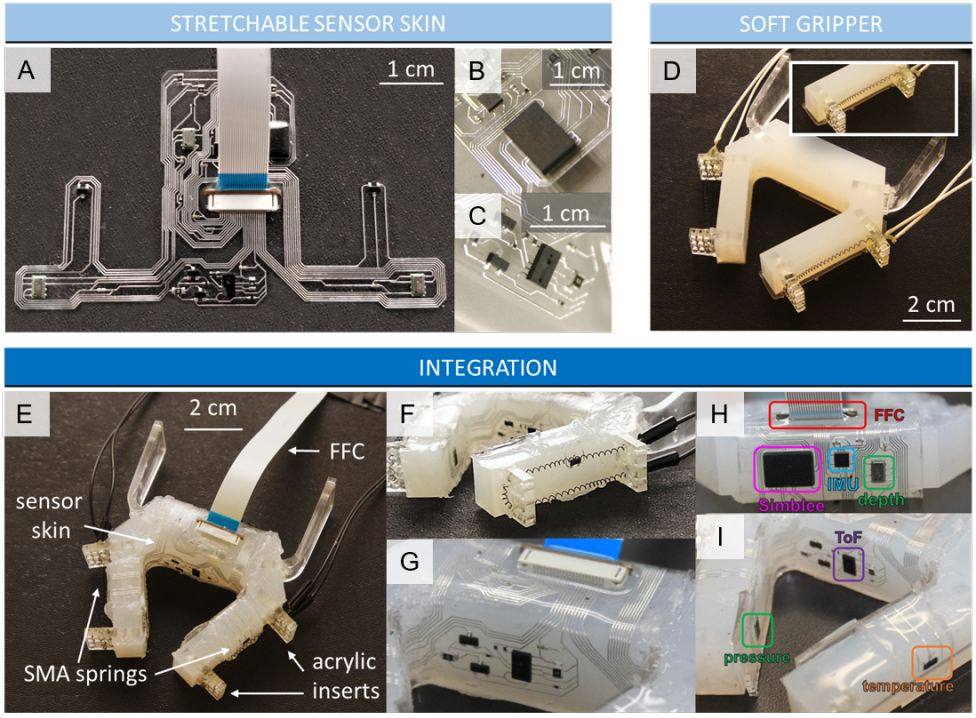

Fig. 2. A) Gripper skin immediately after removal from glass substrate. Close-up views of liquid metal traces surrounding the B) Simblee and C) Time-of-Flight chip. D) Two-finger soft gripper with embedded acrylic inserts and shape-memory springs aligned along each finger. E) Overview of sensorized soft gripper. F) Single shape-memory spring looped through acrylic inserts. G) Close-up view of liquid metal traces bending around sides of the gripper. Labeled H) top-view and F) front-view of the skin electronics.

exploiting the mechanical compliance of nano/microscale thin metal interconnects with serpentine or pre-buckled wavy shapes that deform through flexing or twisting [17]–[20].

An alternative to these approaches employs the use of microfluidic traces of liquid metal (LM) embedded in a soft elastomer [2]. Eutectic Ga-In (EGaIn; 75% Ga and 25% In, by wt.) and Ga-In-Sn (Galinstan; 68% Ga, 22% In, 10% Sn) are particularly attractive because of their high electrical conductivity (3.4×10^6 S/m), low melting point (19°C for Galinstan, 15°C for EGaIn), low viscosity (2 mPa-s), low toxicity [21], negligible vapor pressure [22], [23] and good wetting properties to materials commonly used in IC chip contacts such as gold or copper [12], [24]–[26]. Since these metals are liquid at room temperature and have metallic conductivity, they function as intrinsically stretchable conductors that are not subject to the same limitations of conductive polymers or deterministic architectures. As such, LM-based electronics provide a unique combination of high metallic conductivity and extreme elastomeric stretchability.

Soft systems and electronic skins with embedded LM-based and flex-circuit-based strain [27]–[30], pressure sensors [10], [31]–[33], acceleration, and temperature [34] have already been demonstrated in the literature. However, general soft robotic system integration with more diverse sensing modalities such as orientation and range sensing, and on-board processing capabilities has yet to be shown. Our work closes this gap by introducing a technique for embedding microelectronic sensors and IC chips into a soft and stretchable sensor skin that can then be integrated into a soft robot gripper.

III. DESIGN

We demonstrate successful integration of microelectronic sensors and ICs for applications in soft robotics by introducing a soft gripper that is capable of multi-modal sensing, signal processing, and operation in water. The gripper is actuated using shape memory alloy (SMA) springs that contract when powered with electrical current. The skin contains commercially-available electronic components connected by liquid metal traces sealed in a thin elastomer layer to allow the skin to deform without damaging the circuit (Figure 2A,B,C). The elastomeric gripper contains acrylic inserts that rigidly affix the springs parallel to the fingers (Figure 2D,F). When DC current is passed through the SMA springs, the springs contract due to Joule heating and open the gripper. When DC current is removed the elastomer relaxes, returning the springs to their initial elongated state. The soft gripper is designed to passively hold objects by minimizing activation time in order to conserve the energy required for operation.

The sensorized gripper is composed of a silicone elastomer that is covered with a soft sensing skin and fixed SMA actuators (Figure 2E). The sensor skin is bonded around the gripper and stretches with the movement of the gripper without altering the underlying mechanics. In addition, the elastomer-coated circuit and elastomeric gripper body are not susceptible to galvanic corrosion, making this system ideal for robotic applications in wet environments.

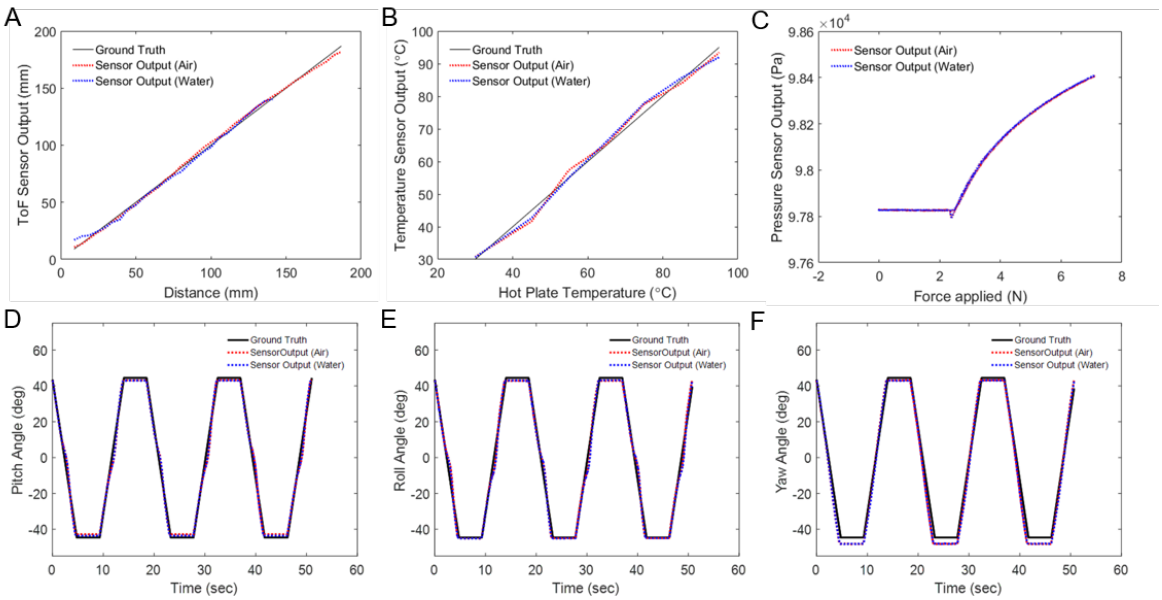

Fig. 3. A) Sensor output vs. actual distance from liquid metal ToF circuit in air and in water. B) Sensor output vs. reference temperature from liquid metal temperature circuit in air and in water. C) Sensor output vs. force applied from the liquid metal pressure circuit in air and in water. Sensor output vs. orientation from the liquid metal IMU circuit in air and in water for D) roll, E) pitch, and F) yaw.

A. *Sensor Skin Fabrication*

The sensor skin includes a processor (Simblee; RFDigital), IMU, ToF chip, three barometric pressure sensors, and two analog temperature sensors. The circuit also contains capacitors, resistors, n-channel MOSFETs, and a 0.5 mm pitch flat flexible cable (FFC) connector. These components were selected in order to provide a variety of sensing modalities during gripping tasks and were placed in locations according to their sensing functionality. The ToF chip is placed in the 'palm' of the gripper to approximate distance to the target and to outline the shape of the target object by scanning (Figure 2G). One pressure sensor is placed in each 'fingertip' to detect contact with an object. The third pressure sensor is placed on the top of the gripper to monitor ambient pressure. The temperature sensors are placed nearest to the SMA springs to estimate their temperature and monitor against overheating. The Simblee and IMU are placed central to the surrounding components (Figure 2H, I). The FFC connector provides power and serial communication with the on-board processor.

The sensor skin is composed of liquid metal traces (width = 200μm) interfaced with several commercially-available sensors (Figure 2B, C) and sealed in polydimethylsiloxane (PDMS; 10:1 base-to-curing agent ratio; Sylgard 184; Dow Corning). Ozutemiz et. al describe this fabrication process in detail in [12]. First, a 20 nm Cr adhesion layer and 100 nm thin film of Cu is sputtered on top of a thin film of cured elastomer. The copper-clad elastomer is patterned using a UV Laser (Protolaser U3; LPKF) and submerged into a bath of 3% NaOH. Then, eutectic gallium-indium (EGaIn) is selectively wetted to the copper traces and the newly coated traces are rinsed with deionized (DI) water and isopropylalcohol (IPA). After the sample is dry, the various electrical components are placed and the circuit is treated with O_2 plasma (Plasma Prep 3; SPI) to improve interfacial bonding. A final sealing layer of PDMS is cast over the device.

B. *Gripper Fabrication*

The soft gripper is fabricated by first preparing the soft silicone (Dragonskin 30; Smooth-On Inc.), which is mixed and defoamed in a planetary centrifugal mixer (AR-100; Thinky) and then degassed in a dessicator for 10 minutes. The main body of the gripper is fabricated by pouring the liquid elastomer in a 3D-printed mold (Objet 24; Stratasys) and curing it in an oven at 70°C for one hour (Figure 2D). Prior to pouring, four acrylic inserts (t=3.175mm) are press-fit into the mold in order to create rigid fixtures to attach the coiled SMA springs (Dynalloy). Two additional acrylic inserts are press-fit as mounting hardware for the robotic arm. The spring wires are 1.37 mm in diameter, 50 mm long fully contracted, and 100 mm long fully elongated. A wire ferrule is crimped on both ends of the SMA spring and adhered to the acrylic insert using a silicone adhesive (Silpoxy; Smooth-On Inc) (Figure 2D). One spring is looped along each finger of the gripper and connected in series to an off-board power supply.

C. *Integration*

For final integration, the completed sensor skin is cut to size and adhered to the soft gripper with a silicone adhesive (Silpoxy; Smooth-On). Weights are placed to ensure maximum surface area contact and the gripper is cured for 24 hours at room temperature. At approximately 1 mm in thickness, the sensor skin is able to wrap around the soft gripper without hindering the mechanics of the shape-memory actuation. The relatively small size of the IC chips

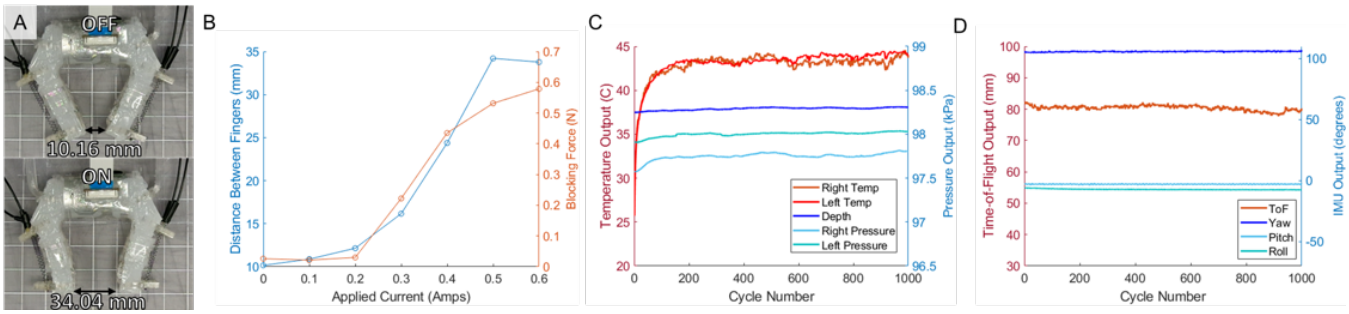

Fig. 4. A) Sensorized soft gripper has a separation of (top) 10.16 mm with the SMA springs relaxed and (bottom) 34.04 mm with the SMA springs activated ($I_{applied} = 0.5A$). B) Separation distance and blocking force vs. applied DC current. C) Outputs of temperature and pressure sensors for 1000 cycles. D) Outputs of ToF and IMU sensors for 1000 cycles.

along with strategic design placement allows the soft robot to integrate a wide variety of sensors without sacrificing its mechanical compliance.

IV. RESULTS AND DISCUSSION

We evaluate the functionality of the individual components of the sensorized soft robot gripper with a series of experiments in dry and wet conditions. We also demonstrate the operation of the sensorized soft robot gripper mounted to the 4-DOF robot arm. From the experimental results, we find that the microelectronic elements operate similar to how they would with a conventional robotic system.

A. Sensors

1) Time-of-Flight: The ToF sensor (VL6180X; ST Microelectronics) measures how long it takes light to travel to the nearest object and reflect back to the sensor and infers distance to a target object from this timing. To characterize the chip, we bonded a liquid metal ToF circuit to a flat surface below a precision measurement stand. Then, we statically measured the distance between the ToF chip and surface of the measurement stand in increments of 5.08 mm (0.2 in), sampling at approximately 20 Hz. The reference distance and measured sensor output is shown in Figure 3A. After linearly fitting the raw sensor output with the ground truth, the model fits the data with an R^2 value of 0.9985 for air and 0.9954 for water. The high R^2 value shows good agreement between the ground truth and the raw measurements. Although the ToF chip was not designed for underwater use, the submerged sensor output converges below 137.16 mm (5.4 in) while the ToF chip in air converges below 177.8 mm (7 in). From these results we conclude that the ToF sensor can be used reliably on LM-based soft circuits both in air and in water up to this range.

2) Temperature: In order to characterize the temperature sensor (MCP9700; Microchip Technology) in air and in water, one liquid metal temperature circuit was placed directly on top of the hot plate, and another was placed in a small jar of water on top of the same hot plate. We sampled both sensors with an Arduino Uno at approximately 10 Hz from 35°C to 95°C in 10°C increments. We waited 2 hours between each data recording to ensure that the temperature had reached equilibrium. As shown in Figure 3B, the sensor performs similarly in water and in air, with a R^2 value of 0.9909 for air and 0.9920 for water from the linear regression. Considering the high R^2 value we conclude that the analog temperature sensor can be used reliably in LM-based soft circuits.

3) Pressure: We performed a compression test using a motorized materials testing system (5959 Dual Column Testing System; Instron) to measure force and sensor output (Figure 3C). The Instron testing system compressed the pressure sensor (MS5607-02BA03; TE Connectivity Measurement Specialties) at a rate of 0.5 mm/min up to 1 mm. We performed this compression test on the liquid metal pressure circuit in both ambient air and submerged in a shallow dish of water. This particular chip does not respond until over 2 N is applied, but behaves similarly in both air and water.

4) Inertial Measurement Unit: We validated the functionality of the liquid metal IMU circuit (MPU9250; InvenSense) by affixing it to a rotating motor mount (AX-12A; Dynamixel) and collecting roll, pitch, and yaw angle measurements in air and in water. Each axis was rotated from 45 to -45 degrees with a constant angular speed of 18 deg/s with 5 second pauses between each half-cycle. The motion profile for each Euler angle (pitch, roll, yaw) is plotted in Figure 3D, E, and F with the corresponding ground truth values for 3 cycles. The results show that the output of the sensor circuit is similar for both in air and in water conditions ($\approx$<1% difference). Compared to the ground truth, there is a maximum of $\approx$4% difference in the pitch and roll angle measurements and $\approx$10% difference in the yaw angle measurement. We attribute these errors to the Mahony filter not accounting for rotational acceleration and the errors in the magnetometer calibration. Nevertheless, the Euler angle estimation errors are within the expected range [35] for the IMU circuit and used sensor fusion algorithm. Thus, we conclude that IMU sensor can be used successfully as integrated into the skin of a soft robot.

B. Gripper

The blocking force and separation distance resulting from different applied currents are reported in Figure 4B. To measure the blocking force of one finger, we mounted the sensorized gripper directly underneath a load cell plate. By

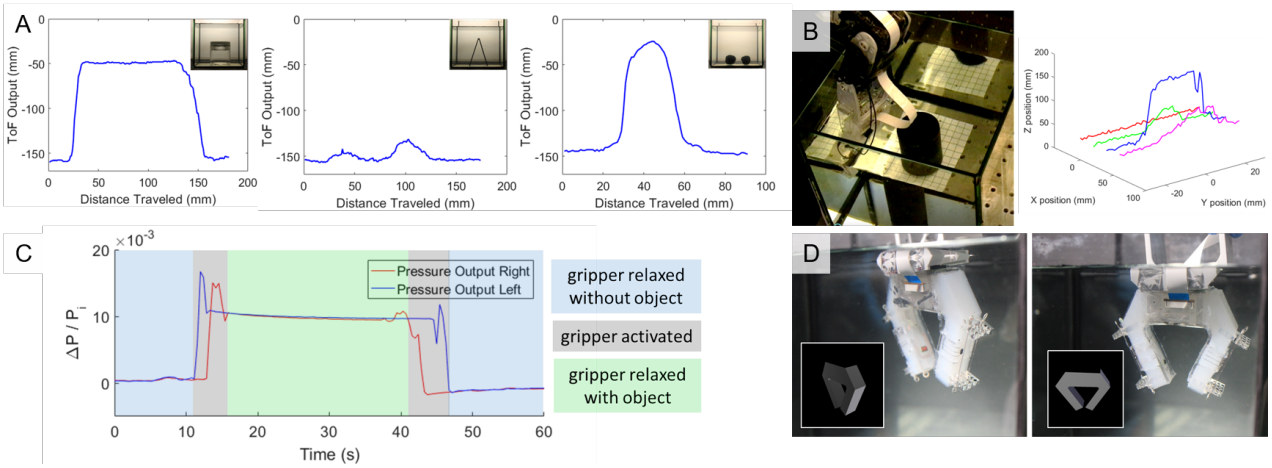

Fig. 5. A) 2D ToF profile scans for a glass jar, triangle, and two moss balls. B) 3D ToF profile scans for a cylindrical object. C) Pressure output for fingertip sensors surrounding a plastic egg. D) Orientation visualization from IMU data.

passing DC current through the SMA coils, the finger starts to push up against the load cell. The maximum force reached within 10 second of activation is considered the blocking force. As seen in Figure 4A, the coils cause the distance between the fingertips to change (≈6% strain in the skin) and allow for a clearance around an object. The initial parting distance was measured as 10.16 mm and the final parting distance was measured as 34.04 mm (Figure 4A). Our experimental results show that the blocking force applied by the gripper increases as the current increases up to a maximum value of ≈0.6 N. In general, the gripper is able to grasp objects around their center of gravity in cases when the maximum fingertip clearance is larger than the object width.

We tested the durability of the sensorized gripper by activating the SMA springs over 1000 cycles. Each cycle included 2 seconds activation (current, I = 0.5A) and 8 seconds of cooling time. All of the sensors were sampled at approximately 2 Hz to ensure proper communication. The results (Figure 4C, D) show that the gripper and sensors continue to function properly throughout without failure. The local temperature increases to approximately 44°C due to their close proximity to the SMA springs.

C. Robotic Arm Demos

We attached the sensorized gripper to a robot arm with four servo motors (AX-12A; Dynamixel). The sensor data is collected and transferred by the on-board microcontroller (Simblee). The 4-DOF arm was programmed to do a 2-D sweep over the length of the tank with different objects placed at the bottom. The general outline of the shape is shown in (Figure 5A). The predicted height (actual height) of the jar was calculated as 110.76 mm (98 mm), the triangle as 118.78 mm (109 mm), and the moss balls (Marimo; Luffy) as 21.77 mm (34 mm) and 8.37 mm (30 mm), respectively. The profile of the moss balls is noticeably noisier because they are located at the limits of the ToF sensor's range (≈150mm). The 4-DOF arm was also programmed to do a 3-D sweep over a 60 by 60 mm area of the tank (Figure 5B). An overview of these demos is also shown in the accompanying video supplement.

The pressure output data for holding a plastic egg, seen in Figure 5C, changes with contact of the object. The first ten seconds of the test are used to determine the initial pressure conditions. There is visible noise associated with the movement of the gripper and activation of the SMA. However, after the SMA relaxes there is a clear increase in pressure from the plastic egg. The delay between the left and right sensors is attributed to small vertical alignment errors during fabrication. In other words, the surface of the object reaches the left pressure sensor first and maintains contact longer than the right pressure sensor. For the IMU, we developed a visualization software in Processing that gives the user an understanding of the current orientation of the gripper (Figure 5D).

V. CONCLUSIONS AND FUTURE WORK

In this study, we have shown that microelectronic sensors and ICs can be successfully integrated into the skin of a soft robot without impairing the functionality of either the robot or the embedded microchips. We demonstrated the fabrication of an SMA actuated soft robotic gripper with an integrated stretchable sensor skin composed of commercially-available electronic components connected by liquid metal traces. We also characterized the operation of each liquid metal sensor circuit in air and water. In conclusion, we demonstrated the functionality of the pressure, ToF, and IMU sensors, and the processor integrated into the stretchable skin of the soft robotic gripper. Although here the sensing skin integration strategy is demonstrated on an SMA-powered soft gripper, the same approach can be used in other soft robotic systems.

Moving forward, we plan to implement a closed-loop control system based on the sensor output data. In addition, we are exploring multi-layer fabrication and functional gradients to reduce the stress concentrations at the PDMS-chip interface, which is where mechanical failure typically

occurs [12], [36]. With the addition of a battery and wireless communication, this approach can be used for untethered soft robots. Using different elastomer substrates, thinner skins, and testing additional off-the-shelf chips would further increase the adaptability of these techniques.

REFERENCES

[1] C. Majidi, "Soft robotics: a perspective – current trends and prospects for the future," *Soft Robotics*, vol. 1, no. 1, pp. 5–11, 2014.

[2] M. L. Hammock, A. Chortos, B. C. K. Tee, J. B. H. Tok, and Z. Bao, "25th anniversary article: The evolution of electronic skin (E-Skin): A brief history, design considerations, and recent progress," *Advanced Materials*, vol. 25, no. 42, pp. 5997–6038, 2013.

[3] N. Lu and D.-H. Kim, "Flexible and Stretchable Electronics Paving the Way for Soft Robotics," *Soft Robotics*, vol. 1, no. 1, pp. 53–62, 2014.

[4] N. Kazem, T. Hellebrekers, and C. Majidi, "Soft multifunctional composites and emulsions with liquid metals," *Advanced Materials*, vol. 29, no. 27, pp. 1 605 985–n/a, 2017, 1605985.

[5] S. Rich, C. Majidi, and R. J. Wood, "Untethered soft robotics," *Nature Electronics*, vol. 1, no. 2, pp. 102–112, 2018.

[6] H. Lee, C. Xia, and N. X. Fang, "First Jump of Microgel: Actuation Speed Enhancement by Elastic Instability," *Soft Matter*, vol. 6, no. 18, p. 4, 2010.

[7] B. Mosadegh, P. Polygerinos, C. Keplinger, S. Wennstedt, R. F. Shepherd, U. Gupta, J. Shim, K. Bertoldi, C. J. Walsh, and G. M. Whitesides, "Pneumatic networks for soft robotics that actuate rapidly," *Advanced Functional Materials*, vol. 24, no. 15, pp. 2163–2170, 2014.

[8] M. T. Tolley, R. F. Shepherd, B. Mosadegh, K. C. Galloway, M. Wehner, M. Karpelson, R. J. Wood, and G. M. Whitesides, "A resilient, untethered soft robot," *Soft Robotics*, vol. 1, no. 3, pp. 213–223, 2014.

[9] V. Arabagi, O. Felfoul, A. H. Gosline, R. J. Wood, and P. E. Dupont, "Biocompatible pressure sensing skins for minimally invasive surgical instruments," *IEEE sensors journal*, vol. 16, no. 5, pp. 1294–1303, 2016.

[10] F. L. Hammond, Y. Menguc, and R. J. Wood, "Toward a modular soft sensor-embedded glove for human hand motion and tactile pressure measurement," *IEEE International Conference on Intelligent Robots and Systems*, pp. 4000–4007, 2014.

[11] B. Shih, D. Drotman, C. Christianson, Z. Huo, R. White, H. I. Christensen, and M. T. Tolley, "Custom Soft Robotic Gripper Sensor Skins for Haptic Object Visualization," 2017.

[12] K. B. Ozutemiz, J. Wissman, O. B. Ozdoganlar, and C. Majidi, "EGaIn-Metal Interfacing for Liquid Metal Circuitry and Microelectronics Integration," *Advanced Materials Interfaces*, vol. 5, no. 10, p. 1701596, 2018.

[13] V. Martinez, F. Stauffer, M. O. Adagunodo, C. Forro, J. Vörös, and A. Larmagnac, "Stretchable Silver Nanowire-Elastomer Composite Microelectrodes with Tailored Electrical Properties." *ACS Applied Materials & Interfaces*, vol. 7, no. 24, pp. 13 467–13 475, 2015.

[14] D. J. Lipomi, M. Vosgueritchian, B. C.-K. Tee, S. L. Hellstrom, J. a. Lee, C. H. Fox, and Z. Bao, "Skin-like pressure and strain sensors based on transparent elastic films of carbon nanotubes." *Nature Nanotechnology*, vol. 6, no. 12, pp. 788–92, 2011.

[15] E. Carone, L. D'Ilario, and A. Martinelli, "New conducting thermoplastic elastomers. I. Synthesis and chemical characterization," *Journal of Applied Polymer Science*, vol. 83, no. 4, pp. 857–867, 2001.

[16] G. Abbati, E. Carone, L. D. Ilario, and A. Martinelli, "Polyurethane Polyaniline Conducting Graft Copolymer with Improved Mechanical Properties," *Journal of Applied Polymer Science*, vol. 89, no. 9, pp. 2516–2521, 2003.

[17] Y. Zhang, S. Wang, X. Li, J. A. Fan, S. Xu, Y. M. Song, K. J. Choi, W. H. Yeo, W. Lee, S. N. Nazaar, B. Lu, L. Yin, K. C. Hwang, J. A. Rogers, and Y. Huang, "Experimental and theoretical studies of serpentine microstructures bonded to prestrained elastomers for stretchable electronics," *Advanced Functional Materials*, vol. 24, no. 14, pp. 2028–2037, 2014.

[18] D.-H. Kim, N. Lu, R. Ma, Y.-S. Kim, R.-H. Kim, S. Wang, J. Wu, S. M. Won, H. Tao, A. Islam, K. J. Yu, T.-i. Kim, R. Chowdhury, M. Ying, L. Xu, M. Li, H.-J. Chung, H. Keum, M. McCormick, P. Liu, Y.-W. Zhang, F. G. Omenetto, Y. Huang, T. Coleman, and J. A. Rogers, "Epidermal electronics," *Science*, vol. 333, no. 6044, pp. 838–843, 2011.

[19] D.-H. Kim, J. Song, W. M. Choi, H.-S. Kim, R.-H. Kim, Z. Liu, Y. Y. Huang, K.-C. Hwang, Y.-w. Zhang, and J. A. Rogers, "Materials and noncoplanar mesh designs for integrated circuits with linear elastic responses to extreme mechanical deformations." *Proceedings of the National Academy of Sciences of the United States of America*, vol. 105, no. 48, pp. 18 675–18 680, 2008.

[20] S. P. Lacour, J. Jones, S. Wagner, T. Li, and Z. Suo, "Stretchable Interconnects for Elastic Electronic Surfaces," *Proceedings of the IEEE*, vol. 93, no. 8, pp. 1459–1466, 2005.

[21] Y. Lu, Q. Hu, Y. Lin, D. B. Pacardo, C. Wang, W. Sun, F. S. Ligler, M. D. Dickey, and Z. Gu, "Transformable liquid-metal nanomedicine," *Nature Communications*, vol. 6, no. 10066, p. 10066, 2015.

[22] M. D. Dickey, R. C. Chiechi, R. J. Larsen, E. A. Weiss, D. A. Weitz, and G. M. Whitesides, "Eutectic gallium-indium (EGaIn): A liquid metal alloy for the formation of stable structures in microchannels at room temperature," *Advanced Functional Materials*, vol. 18, no. 7, pp. 1097–1104, 2008.

[23] I. D. Joshipura, H. R. Ayers, C. Majidi, and M. D. Dickey, "Methods to pattern liquid metals," *Journal of Materials Chemistry C*, vol. 3, no. 16, pp. 3834–3841, 2015.

[24] J. Wissman, M. D. Dickey, and C. Majidi, "Field-controlled electrical switch with liquid metal," *Advanced Science*, vol. 4, no. 12, pp. 1 700 169–n/a, 2017, 1700169.

[25] A. Hirsch, H. O. Michaud, A. P. Gerratt, S. de Mulatier, and S. P. Lacour, "Intrinsically stretchable biphasic (solidliquid) thin metal films," *Advanced Materials*, vol. 28, no. 22, pp. 4507–4512, 2016.

[26] M. R. Khan, C. B. Eaker, E. F. Bowden, and M. D. Dickey, "Giant and switchable surface activity of liquid metal via surface oxidation," *Proceedings of the National Academy of Sciences*, vol. 111, no. 39, pp. 14 047–14 051, 2014.

[27] J. T. Muth, D. M. Vogt, R. L. Truby, Y. Mengüç, D. B. Kolesky, R. J. Wood, and J. a. Lewis, "Embedded 3D printing of strain sensors within highly stretchable elastomers," *Advanced Materials*, pp. 6307–6312, 2014.

[28] Y. Menguc, Y.-L. Park, H. Pei, D. Vogt, P. M. Aubin, E. Winchell, L. Fluke, L. Stirling, R. J. Wood, and C. J. Walsh, "Wearable soft sensing suit for human gait measurement," *The International Journal of Robotics Research*, vol. 33, no. 14, pp. 1748–1764, 2014.

[29] R. Adam Bilodeau, E. L. White, and R. K. Kramer, "Monolithic fabrication of sensors and actuators in a soft robotic gripper," *IEEE International Conference on Intelligent Robots and Systems*, vol. 2015-December, pp. 2324–2329, 2015.

[30] E. L. White, J. C. Case, and R. K. Kramer, "Multi-mode strain and curvature sensors for soft robotic applications," *Sensors and Actuators, A: Physical*, vol. 253, pp. 188–197, 2017.

[31] Y.-L. Park, C. Majidi, R. Kramer, P. Bérard, and R. J. Wood, "Hyperelastic pressure sensing with a liquid-embedded elastomer," *Journal of Micromechanics and Microengineering*, vol. 20, no. 12, p. 125029, 2010.

[32] J. H. Low, W. W. Lee, P. M. Khin, N. V. Thakor, S. L. Kukreja, H. L. Ren, and C. H. Yeow, "Hybrid Tele-Manipulation System Using a Sensorized 3-D-Printed Soft Robotic Gripper and a Soft Fabric-Based Haptic Glove," *IEEE Robotics and Automation Letters*, vol. 2, no. 2, pp. 880–887, 2017.

[33] V. Wall, G. Zoller, and O. Brock, "A method for sensorizing soft actuators and its application to the RBO hand 2," *2017 IEEE International Conference on Robotics and Automation (ICRA)*, pp. 4965–4970, 2017.

[34] S. Xu, Y. Zhang, L. Jia, K. E. Mathewson, K.-I. Jang, J. Kim, H. Fu, X. Huang, P. Chava, R. Wang, S. Bhole, L. Wang, Y. J. Na, Y. Guan, M. Flavin, Z. Han, Y. Huang, and J. A. Rogers, "Soft microfluidic assemblies of sensors, circuits, and radios for the skin," *Science*, vol. 344, no. 6179, pp. 70–74, 2014.

[35] T. Michel, H. Fourati, P. Genevs, and N. Layada, "A comparative analysis of attitude estimation for pedestrian navigation with smartphones," in *2015 International Conference on Indoor Positioning and Indoor Navigation (IPIN)*, Oct 2015, pp. 1–10.

[36] N. Naser, L. P. R., and F. G. K., "Material gradients in stretchable substrates toward integrated electronic functionality," *Advanced Materials*, vol. 28, no. 18, pp. 3584–3591. [Online]. Available: https://onlinelibrary.wiley.com/doi/abs/10.1002/adma.201505818